Evaluation of optical and microwave-derived vegetation indices for monitoring aboveground biomass over China

Zhongbing Chang, Lei Fan, Jean-Pierre Wigneron, Ying-Ping Wang, Xiaojun Li, Mengjia Wang, Xiangzhuo Liu, Huan Wang, Tianxiang Cui, Ling Yu, et al.

HAL Id: hal-04643906
https://hal.inrae.fr/hal-04643906

Submitted on 10 Jul 2024

Evaluation of optical and microwave-derived vegetation indices for monitoring aboveground biomass over China

Zhongbing Chang, Lei Fan, Jean-Pierre Wigneron, Ying-Ping Wang, Xiaojun Li, Mengjia Wang, Xiangzhuo Liu, Huan Wang, Tianxiang Cui, Ling Yu, Jianping Wu, Xin Xiong, Shuo Zhang, Xuli Tang & Junhua Yan

View supplementary material

Published online: 21 Mar 2024.

Submit your article to this journal

Article views: 901

View related articles

View Crossmark data

Taylor & Francis
Taylor & Francis Group

Evaluation of optical and microwave-derived vegetation indices for monitoring aboveground biomass over China

Zhongbing Chang [a], Lei Fan [b], Jean-Pierre Wigneron [c], Ying-Ping Wang [d], Xiaojun Li[c], Mengjia Wang[c], Xiangzhuo Liu[c], Huan Wang[c], Tianxiang Cui[e], Ling Yu[b], Jianping Wu[f], Xin Xiong[g], Shuo Zhang[h], Xuli Tang[i] and Junhua Yan [i]

[a]Key Laboratory of Natural Resources Monitoring in Tropical and Subtropical Area of South China, Ministry of Natural Resources, Surveying and Mapping Institute Lands and Resource Department of Guangdong Province, Guangzhou, China; [b]Chongqing Jinfo Mountain Karst Ecosystem National Observation and Research Station, School of Geographical Sciences, Southwest University, Chongqing, China; [c]ISPA, UMR 1391, INRAE Nouvelle-Aquitaine Bordeaux, Villenave d'Ornon, France; [d]CSIRO Oceans and Atmosphere, Melbourne, Australia; [e]College of Forestry, Nanjing Forestry University, Nanjing, Jiangsu, China; [f]Guangdong Provincial Key Lab of Remote Sensing and Geographical Information System, Guangzhou Institute of Geography, Guangdong Academy of Sciences, Guangzhou, China; [g]Lushan Botanical Garden, Chinese Academy of Sciences, Jiujiang, China; [h]Center for Zhaoqing High-level Talent Development, Zhaoqing Municipal Bureau of Forestry, Zhaoqing, China; [i]Key Laboratory of Vegetation Restoration and Management of Degraded Ecosystems, South China Botanical Garden, Chinese Academy of Sciences, Guangzhou, China

ABSTRACT

The microwave-derived vegetation optical depth (VOD) products were used to monitor aboveground biomass (AGB) at regional to global scales, but the ability of VOD to monitor AGB in China is uncertain. This study evaluated the sensitivity of four VOD products (e.g. L-VOD, IB-VOD, LPDR-VOD, and Liu-VOD) and optical vegetation indices (VI) (e.g. NDVI, EVI, LAI, and tree cover from MODIS) to the AGB across China. Our results showed tree cover product has the highest spatial agreement with reference AGBs (indicated by the median correlation value of 0.85), followed by L-VOD (with a median correlation value of 0.80), which performs better than other VIs and VODs. Further comparisons between reference and estimated AGB computed using the fitted logistic regression showed that AGB estimations from tree cover and L-VOD outperformed the estimations from other VIs and VODs over most vegetation types (except forest), indicated by the higher median correlation value of 0.86 and 0.83 and lower *RMSD* of 23.9 and 27.3 Mg/ha, respectively. The good performance of tree cover could be partly due to that tree cover product is not independent from the reference AGBs. The good performance of L-VOD can be explained by its higher sensitivity to the vegetation characteristics of the entire canopy (including woody component), relative to other VODs and VIs. Among the six reference AGB products, Saatchi-WT and Saatchi-RF products were found to have the best correlations with VIs and VODs. This study demonstrates that microwave VODs, particularly L-VOD, are effective proxies for large-scale monitoring of vegetation AGB in China.

1. Introduction

Aboveground biomass (AGB) serves as a crucial proxy for productivity, carbon sequestration and carbon balance capacity in terrestrial ecosystems (Houghton 2005; Scholze et al. 2017). Accurate estimation of AGB in terrestrial ecosystems is essential to accurately quantify carbon emissions and removals resulting from land use and climate change (Harris et al. 2021; Li et al. 2017; Yang et al. 2022). China's forest coverage has achieved 22.96%, and plays a significant role in the global carbon balance in terms of both carbon emissions and uptake (Jiang et al. 2022; Piao et al. 2009; Zhou et al. 2019). It is therefore critical to monitor the AGB stocks and its dynamics in China to mitigate climate change (Fang et al. 2018; Piao et al. 2022).

Remote sensing techniques that integrate multi-source remote sensing datasets can greatly enhance the efficiency and precision of AGB mapping on a large scale (Harris et al. 2021; Rodriguez-Veiga et al. 2019; Xiao et al. 2019). Remote sensing datasets from optical, synthetic aperture radar (SAR), and light detection and ranging (LiDAR) have become a prevalent approach for AGB mapping (Chen et al. 2023; Huang et al. 2022; Saatchi et al. 2011; Su et al. 2016; Yang et al. 2023). Although LiDAR is considered as the most promising method for estimating AGB, there was no dedicated spaceborne LiDAR designed specifically to estimate vegetation AGC until the launch of Global Ecosystem Dynamics Investigation in 2019 (Wang et al. 2023). Among various remote sensing datasets, the optical vegetation indices (VIs)

(e.g. NDVI, EVI, and LAI) are frequently utilized as proxy for AGB monitoring (Xu et al. 2021; Zhang et al. 2019), because VIs are calculated based on the spectral response of the vegetation and therefore can be used as an indirect indicator of AGB (Blackard et al. 2008; Myneni et al. 2001; Xu et al. 2020). VIs could provide better spatial coverage with high resolution and are available for long-term time series, which can provide effective global monitoring of vegetation trends (J. M. Chen et al. 2019; Qin et al. 2023). However, the optical VIs are known to be affected by clouds and aerosols, and suffered from the signal saturation problem in dense vegetation areas (Liao et al. 2020; Myers-Smith et al. 2020). Moreover, the retrieved AGB values using these approaches are generally available for only a single epoch, and therefore cannot be used to monitor the temporal dynamics of AGB stocks (Brandt et al. 2018; Fan et al. 2019).

The vegetation optical depth (VOD), retrieved from satellite passive microwaves and directly proportion to the vegetation water content, provides independent data to monitor AGB dynamics at regional to global scales (Fan et al. 2019; Jones et al. 2011; Li et al. 2021; Liu et al. 2015; Wigneron et al. 2021). Compared to optical VIs, VOD is sensitive to vegetation characteristics of both leafy and woody components, and is mostly insensitive to atmospheric and cloud effects, thus is more sensitive to AGB (Dou et al. 2023; Wigneron et al. 1993; Zhao et al. 2021). AGB stocks have been monitored using VOD products from multiple microwave sensors, including the first long-term global VOD product (hereafter Liu-VOD) (Liu et al. 2015), and the global land parameter data record (LPDR) X-band (10.7 GHz) VOD (hereafter LPDR-VOD) (Du et al. 2017). Although the P-band microwave shows high sensitivity to AGB even in densely forests, there are still no available spaceborne P-band radar until the launch of Biomass mission scheduled in 2024 (Quegan et al. 2019). The Chinese Terrestrial Water Resources Satellite (TWRS) at L-band is under development, will provide global vegetation water content and soil moisture by combining L-band active and passive microwave (Zhao et al. 2020). Recently, VOD at L-band (1.4 GHz) (L-VOD), derived from low-frequency passive microwave satellite Soil Moisture and Ocean Salinity (SMOS), has been established as a promising index for monitoring the AGB dynamics over tropics (Brandt et al. 2018; Fan et al. 2023; Tong et al. 2020; Wigneron et al. 2020). This is due to the microwave observation at L-band has a stronger penetration capacity because of the long wavelength, is thus less sensitive to saturation effects (Fan et al. 2019), relative to high-frequency VOD products.

Assessing the sensitivity of VIs and VODs products to AGB is a first and necessary step before using them in monitoring AGB dynamics over China. The performance of VODs products have been evaluated over tropical regions (Chaparro et al. 2019; Gevaert et al. 2016; Rodríguez-Fernández et al. 2018; Teubner et al. 2018) or on a limited frequency (Grant et al. 2016; Lawrence et al. 2014; Li et al. 2020; Mialon et al. 2020; Vittucci et al. 2019). However, the performance of VODs has not been quantified in China. For example, the radio frequency interferences (RFI) have a significant impact on L-VOD measurements in China, which could decrease the performance of L-VOD on monitoring AGB in China (Chang et al. 2023; Wigneron et al. 2021). Although LPDR-VOD and Liu-VOD are less affected by RFI, they could have saturation issue over the dense forests (Prigent and Jimenez 2021; Schmidt et al. 2023). Recently, an alternative X-band VOD product, developed by INRAE Bordeaux (hereafter IB-VOD) (Wang et al. 2021), have not yet assessed or comparative analyzed in China. Thus, further work is needed to quantify and compare the sensitivity of VODs to AGB at different frequencies and for different land cover classes in China.

Therefore, the objective of this study is to assess the performance of four VOD products (e.g. L-VOD, IB-VOD, LPDR-VOD, and Liu-VOD) and four optical VIs (e.g. NDVI, EVI, LAI, and tree cover) on monitoring AGB across China.

2. Data

2.1. Microwave VOD products

2.1.1. L-VOD
The L-VOD was retrieved from the SMOS satellite using the SMOS-IC (INRA-CESBIO) algorithm (version 105) (Fan et al. 2019; Wigneron et al. 2017). The L-VOD product was retrieved by the L-band (1.4 GHz) microwave emission of the biosphere (L-MEB) model, providing daily global VOD and soil moisture (SM) dataset at a resolution of 0.25° for 2010–2021. In this study, the root mean square error between the measured and simulated brightness temperature associated with the L-VOD product was used to filter out observations affected by RFI. Refer to Fan et al. (2019), observations affected by RFI larger than 10K were filtered out. In addition, observations with a strong topography, frozen conditions, and the sum of water, urban and ice fractions higher than 10% were excluded (Fernandez-Moran et al. 2017). The SMOS-IC VOD product was selected because it has been shown to exhibit a stronger relationship with AGB than other SMOS products (Li et al. 2021; Rodríguez-Fernández et al. 2018).

2.1.2. IB-VOD
The IB-VOD product was retrieved from AMSR2 X-band (10.7 GHz) descending data, using X-MEB (X-band microwave emission of the biosphere)

model (Wang et al. 2021), with a spatial resolution of 0.25°. The X-MEB model is an extension of the L-MEB model (Fernandez-Moran et al. 2017; Wigneron et al. 2007), and the values of the soil and vegetation parameters were calibrated for X-band. The IB-VOD showed competitive advantages with other X-VOD products and higher spatial and temporal correction than LAI or NDVI (Schmidt et al. 2023; Wang et al. 2021).

2.1.3. LPDR-VOD

The LPDR-VOD was derived from the land parameter data record (LPDR, version 2), which was retrieved from AMSR-E and AMSR2 sensors at 10.7 GHz based on both ascending (13.30) and descending (01.30) data (Du et al. 2017). The LPDR provides a long-term (2002–2021) global record of key environment variables which including daily X-VOD (10.7 GHz) products at 0.25° resolution. The grid cells affected by frost conditions, large water bodies, strong precipitation or RFI were excluded using the quality assessment (QA) files (Kim et al. 2017).

2.1.4. Liu-VOD

The Liu-VOD was retrieved from three passive microwave instruments: Special Sensor Microwave Imager (SSM/I), TRMM Microwave Imager (TMI) and AMSR-E, using the land parameter retrieval model (LPRM) (Liu et al. 2011). This product provides a continuous long-time series from 1993 to 2012 at 0.25° resolution. The VOD values affected by open water bodies and frost conditions were corrected to improve the data quality (Liu et al. 2015).

2.2. Optical vegetation indices

We applied four optical VIs in this study that are commonly used to estimate AGB in the previous studies (Table 1), including:

(1) NDVI and EVI, provided by the monthly MODIS product (MOD13A3) at 1 km spatial resolution (Didan 2015), used as proxy for green vegetation cover (Hmimina et al. 2013;

Huete et al. 2002) and biomass (Chen et al. 2023; Myneni et al. 2001; Zhang et al. 2022).

(2) LAI, derived from 8-day MODIS product (MOD15A2) at 500 m spatial resolution (R. Myneni, Knyazikhin, and Park 2015), providing information on the amount and distribution of vegetation and its ability to exchange carbon, water, and energy with the atmosphere (Chen and Black 1992).

(3) Tree cover, derived from the MOD44B vegetation continuous fields (VCF) product, with a spatial resolution of 250 m (Dimiceli et al. 2015). It was measured as the percentage of skylight blocked by trees that are at least 5 m (Hansen et al. 2003).

To reduce the impact of different temporal coverages and gaps between the reference AGB and VIs/VODs, the relationships between AGB and VODs/VIs were compared using the average value of VIs/VODs. The pixels affected by snow/ice, cloud cover, and non-land were filtered using the quality assessment (QA) layer accompanying the product. All VI products were aggregated to 0.25° through simple averaging to match the spatial resolution of VODs.

2.3. Aboveground biomass

This study used six AGB benchmark maps to assess the sensitivity of VIs and VODs to AGB (Table 1), including:

(1) Saatchi map, provides the AGB density for the pan-tropics at 1 km resolution for the early 2000s (Saatchi et al. 2011). An updated version of global AGB density map for 2015 was used in this study (Carreiras et al. 2017).

(2) Baccini map, provides the AGB estimates for the pan-tropics at 500 m resolution (Baccini et al. 2012). An updated version that expands on the methodology presented in Baccini et al. (2012) and presents global biomass density at approximately 30 m resolution was used in this study (Baccini et al. 2017).

Table 1. Overview of the VODs, VIs, and reference AGB datasets used in this study.

Dataset	Products/Sensor	Period	Spatial resolution	Reference
L-VOD	SMOS-IC V105	2013–2017	0.25°	Fan et al. (2019)
IB-VOD	AMSR2	2013–2017	0.25°	M. Wang et al. (2021)
LPDR-VOD	AMSR-E and AMSE2	2013–2017	0.25°	Du et al. (2017)
Liu-VOD	SSM/I,AMSR-E, MWRI, and Windsat	2008–2012	0.25°	Liu et al. (2015)
NDVI	MOD13A3	2013–2017	1 km	Didan (2015)
EVI	MOD13A3	2013–2017	1 km	Didan (2015)
LAI	MOD15A2	2013–2017	500 m	R. Myneni et al. (2015)
Tree Cover	MOD44B	2013–2017	250 m	Dimiceli et al. (2015)
Saatchi	–	2015	1 km	Saatchi et al. (2011)
Baccini	–	2007	30 m	Baccini et al. (2012)
CCI	–	2017	100 m	Santoro et al. (2021)
Saatchi-WT	–	2010s	1 km	Chang et al. (2021)
Saatchi-RF	–	2010s	1 km	Chang et al. (2021)
Su	–	2004	1 km	Su et al. (2016)

(3) CCI map, presents a global map of AGB at 100 m resolution for 2017 (Santoro et al. 2022). The CCI map was derived from a combination of multiple SAR observations (Sentinel-1, ALOS, and PALSAR).

(4) Saatchi-WT map, produced by merging the forest AGB map and non-forest AGB map (Supplementary Text) (Chang et al. 2021). The forest AGB map was estimated using the weighting technique (WT) method to merge the five published AGB products (Baccini et al. 2012; Huang et al. 2019; Saatchi et al. 2011; Santoro et al. 2021; Su et al. 2016). Non-forest AGB map was from Saatchi map over non-forest regions.

(5) Saatchi-RF map, similar to Saatchi-WT map, produced by merging the forest AGB map and non-forest AGB map. The forest AGB map was estimated based on the same datasets in WT map, but using random forest (RF) regression method (Supplementary Text) (Chang et al. 2021).

(6) Su map, estimating AGB in China forest at 1 km resolution for 2004 (Su et al. 2016). The Su map was derived from a combination of LiDAR, optical imagery, and ground inventory data using random forest method.

These AGB products constituted the best benchmarks to date and have been used as benchmark maps for monitoring the AGB dynamics over the global and tropics regions (Brandt et al. 2018; Fan et al. 2023; Qin et al. 2021). In this study, the spatial resolution of all AGB maps were aggregated to 0.25° through simple averaging.

2.4. Land cover

The European Space Agency's (ESA's) Climate Change Initiative (CCI) L4 land cover data (ESA. 2017) for 2015 was aggregated from 300 m to 0.25° by dominant class. We reclassified the land cover data into four classes (Figure S1 and Table S1), namely forest, shrubland, grassland, and cropland.

3. Methods

The reference AGB datasets were acquired from years 2000 to 2015 (Table 1). Given the different temporal coverages and gaps between the reference AGB and VOD datasets, the relationships between AGB and VOD were estimated by comparing the reference AGBs with (1) the average value of L-VOD, IB-VOD, and LPDR-VOD during 2013–2017, (2) the average value of Liu-VOD during 2008–2012. Our study focused on carbon stocks in vegetation biomes, so we masked the non-vegetated pixels dominated by "settlement", "water", "bare and spare vegetation", and "wetland".

To ensure the relatively homogeneous land cover conditions, only pixels with a dominant fraction of single class higher than 80% are considered. To understand the sensitivity of VIs and VODs to AGB over the different land cover types, the relationships between reference AGBs and VIs/VODs with were analyzed for forest, shrubland, grassland, and cropland, respectively.

The relationship of VIs and VODs to AGB was indicated by the spatial correlation (R_1) calculated by comparing the AGB datasets with VIs and VODs using the Pearson correlation coefficient (Entekhabi et al. 2010), defined as follows:

$$R_1 = \frac{\sum \left(VOD - \overline{VOD}\right)\left(AGB_{ref} - \overline{AGB}_{ref}\right)}{\sqrt{\sum \left(VOD - \overline{VOD}\right)^2 \sum \left(AGB_{ref} - \overline{AGB}_{ref}\right)^2}}$$

(1)

where VOD and AGB_{ref} is the values of VOD and reference AGB. $\overline{VOD}$ and $\overline{AGB}_{ref}$ is the average values of VOD and reference AGB. The p-value (0.05) was used to define the significance level of the correlation.

The regression relationship between VOD and AGB were established by empirical functions, including the linear (Brandt et al. 2018), arctangent (Liu et al. 2015; Qin et al. 2021), and logistic regressions (Rodríguez-Fernández et al. 2018). The linear and arcangent regressions were used to assess the carbon dynamic in tropical regions. We utilized a logistic regression equation to establish the relationship between the VIs/VODs and AGB (Fan et al. 2023):

$$AGB = \frac{a}{1 + e^{-b(VOD-c)}} + d$$

(2)

where a, b, c, and d are regression parameters.

We applied the logistic regression (Equation (2)) with the fitted parameters (Table S2) to VOD products to estimate VOD-based AGB density (Mg/ha). Spatial correlation (R_2) and root mean square deviation ($RMSD$), computed between estimated and reference AGBs, are used to assess the precision of AGB estimations retrieved from various VIs and VODs products.

$$R_2 = \frac{\sum \left(AGB_{ref} - \overline{AGB}_{ref}\right)\left(AGB_{estimate} - \overline{AGB}_{estimate}\right)}{\sqrt{\sum \left(AGB_{ref} - \overline{AGB}_{ref}\right)^2 \sum \left(AGB_{estimate} - \overline{AGB}_{estimate}\right)^2}}$$

(3)

$$RMSD = \sqrt{\frac{\sum \left(AGB_{ref} - AGB_{estimate}\right)^2}{N}}$$

(4)

where AGB_{ref} and $AGB_{estimate}$ is the value of reference and estimated AGB. $\overline{AGB}_{ref}$ and $\overline{AGB}_{estimate}$ is the average values of reference and estimated AGB. All the above defined statistical metrics (R_1, R_2, and $RMSD$) were calculated using the overlapping pixels (including 8302 pixels covering 5.19 million km^2) for VI and VOD products.

4. Results

4.1. Spatial patterns of VODs, VIs, and AGB products

Our results showed that the spatial distribution of All VODs closely matches the distribution of VIs (Figure 1 (a–f)). The highest VOD values are found in forests from southern and northeastern China, while the VOD values in temperate steppe/desert and Qinghai-Tibet plateau alpine vegetation are generally low. The same pattern can be observed in the reference AGB maps and the spatial patterns of all AGB estimates are quite similar (Figure 2(a–f)).

4.2. Relationship between VIs/VODs and AGB

4.2.1. The whole biomes

The spatial correlations (R_1) between VIs/VODs and AGB, as estimated by six reference AGB maps, are summarized in Table 2. The density scatter plots are
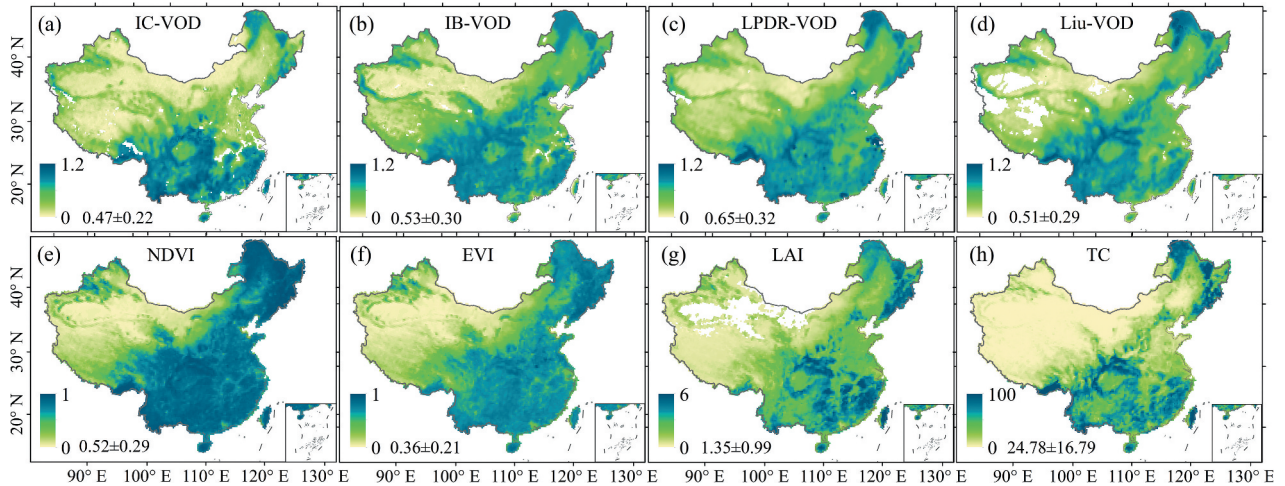

Figure 1. Spatial patterns of the VOD and VI maps over China. (a) SMOS-IC L-VOD, (b) IB X-VOD, (c) LPDR X-VOD, (d) liu-VOD, (e) NDVI, (f) EVI, (g) LAI, (h) tree cover. The numbers represents the mean ± SD of each product. Map review number: No. GS(2022) 1561. Note that large differences in these six reference AGB estimates can be observed over the whole China (Table S3). For example, Saatchi map has the largest forest and shrubland AGB carbon stock values (11.49 Pg C for forest and 3.33 Pg C for shrubland), while CCI map has the largest grassland and cropland AGB carbon stock values (2.81 Pg C for grassland and 1.83 Pg C for cropland). On the contrary, the lowest AGB carbon stock values are from CCI map in forest (7.19 Pg C) and shrubland (2.45 Pg C), from Baccini map in grassland (0.47 Pg C) and cropland (0.43 Pg C), respectively. In consideration of the forest carbon stock in benchmark AGC maps (Table S3), the values range from 7.19 Pg C (CCI) to 11.49 Pg C (Saatchi). Considering these six reference AGB maps contain uncertainties and bias, and none can be considered reliable (Fan et al. 2019). Refer to the previous study, the median of these six maps were used to assess the relationships of VOD/VIs and AGB to avoid the potential uncertainties from a single AGB reference map (Cui et al. 2023; Rodríguez-Fernández et al. 2018).
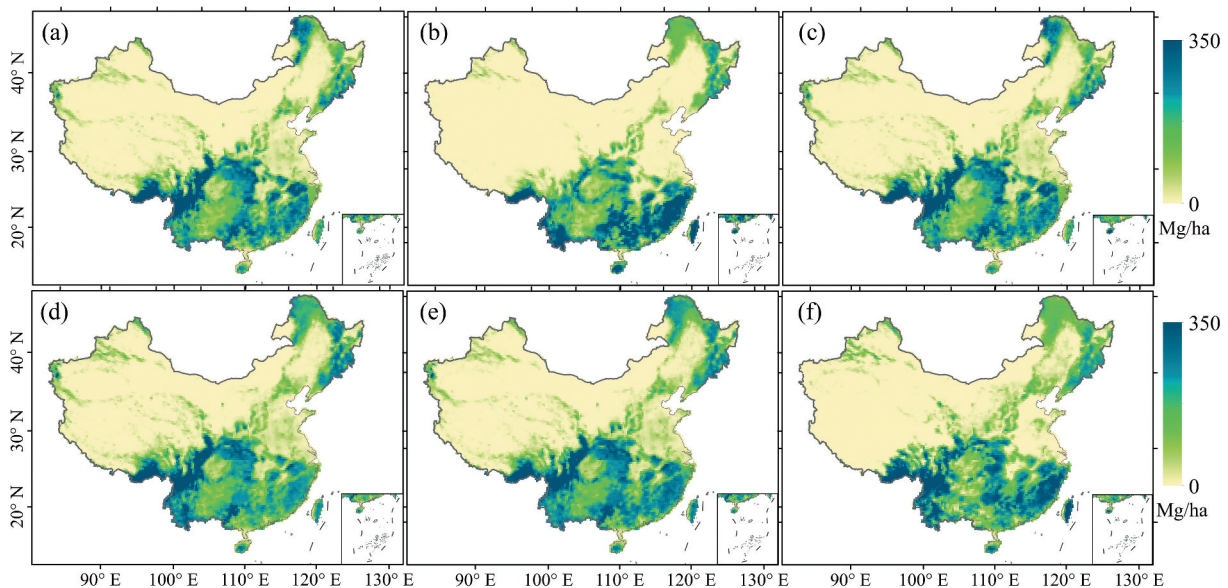

Figure 2. Spatial patterns of the six reference AGB maps over China. (a) Saatchi, (b) Baccini, (c) CCI, (d) Saatchi-WT, (e) Saatchi-RF, and (f) su. Map review number: No. GS(2022)1561.

Table 2. Spatial correlation (R_1) between VIs/VODs and reference AGBs. All the correlations are significant considering the criteria $p < 0.05$.

Products	L-VOD	IB-VOD	LPDR-VOD	Liu-VOD	NDVI	EVI	LAI	Tree Cover
Saatchi	0.78	0.71	0.77	0.76	0.58	0.53	0.71	0.86
Baccini	0.78	0.63	0.71	0.65	0.54	0.53	0.75	0.84
CCI	0.79	0.64	0.70	0.70	0.49	0.47	0.60	0.79
Saatchi-WT	0.83	0.74	0.81	0.79	0.63	0.59	0.74	0.90
Saatchi-RF	0.85	0.76	0.83	0.81	0.65	0.62	0.78	0.92
Su	0.76	0.70	0.73	0.72	0.56	0.52	0.69	0.82

presented in Figure 3 (with Saatchi) and Figure S2 (with Baccini, CCI, Saatchi-WT, Saatchi-RF, and Su). Overall, all the scatter plots show a non-linear relationship between VIs/VODs and reference AGBs.

Considering the sensitivity of VIs to AGB, the highest correlation values were obtained for tree cover product ($R_1 = 0.79$–0.92), followed by LAI ($R_1 = 0.60$–0.78), while NDVI and EVI showed the lowest correlation with reference AGBs ($R_1 = 0.49$–0.65 for NDVI and $R_1 = 0.47$–0.62 for EVI) (Table 2). It can be seen that the VIs such as NDVI and EVI saturate obviously along AGB values increasing sharply from 50 to 300 Mg/ha (Figure 3(e,f) and Figure S2(e,f)). Compared with other VIs, the relationship between tree cover and reference AGBs can be observed to be almost linear (Figure 3(h) and Figure S2(h)), suggesting a good spatial agreement between tree cover product and reference AGBs.

With respect to VODs, L-VOD presented the highest correlation with reference AGBs ($R_1 = 0.76$–0.85), followed by LPDR-VOD ($R_1 = 0.70$–0.83), Liu-VOD ($R_1 = 0.65$–0.81), and IB-VOD ($R_1 = 0.63$–0.76)

(Table 2). The scatterplots between L-VOD and reference AGBs showed a relatively higher dispersion when AGB >150 Mg/ha (Figure 3(a) and Figure S2(A)). For IB-VOD and LPDR-VOD, both of them trended to saturate with AGB values higher than 100 Mg/ha (Figures 3(b–f) and Figure S2(b,c)). The scatterplots between Liu-VOD and reference AGBs showed a higher dispersion for high VOD values (~0.8), with AGB values spanning a range from 100 to 300 Mg/ha (Figure 3(d) and Figure S2(d)). In summary, IB-VOD, LPDR-VOD and Liu-VOD presented saturation signals when AGB values are higher than 100 Mg/ha. L-VOD showed a higher spatial correlation to AGB, without strong signs of saturation, compared with IB-VOD, LPDR-VOD and Liu-VOD.

We computed the spatial correlations (R_2) between reference AGBs and the AGBs estimated using the fitted logistic regression (Equation (2)) and calibrated parameters (Table S2). Overall, AGBs retrieved using tree cover product showed the best agreement with reference AGBs, with a median R_2 value of 0.86
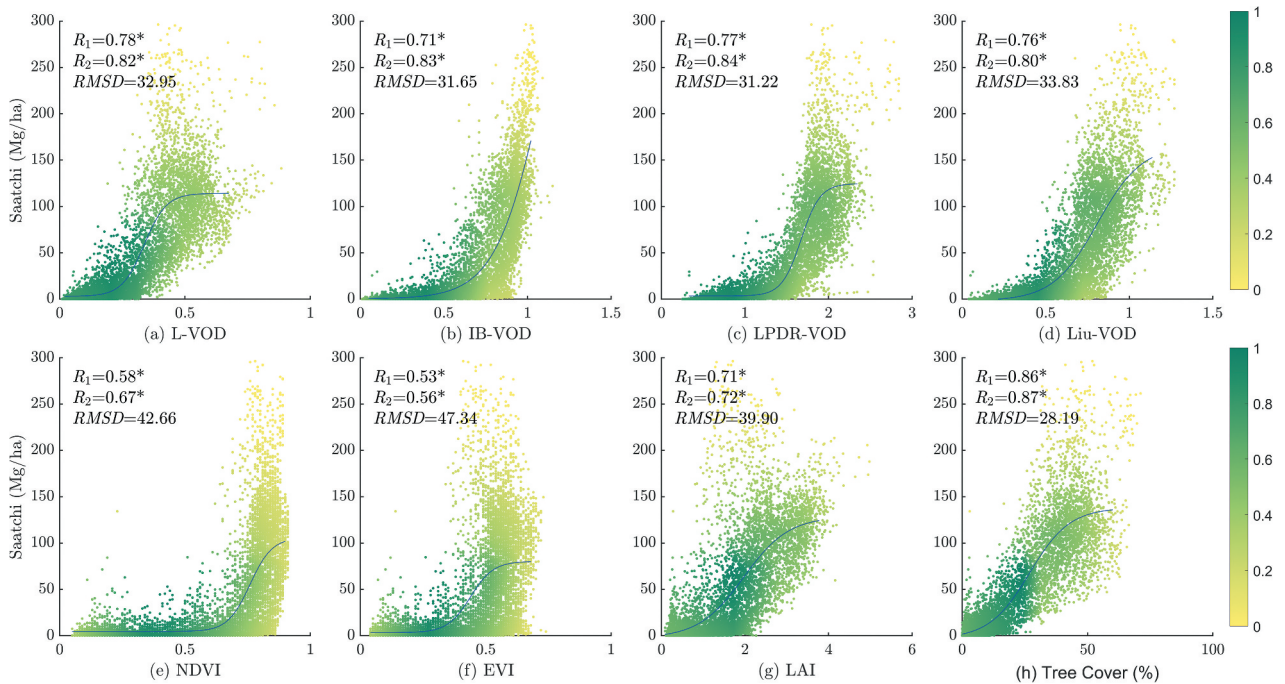
Figure 3. The spatial relationship (R_1, R_2, and *RMSD* (Mg/ha)) between Saatchi AGB and VIs/VODs from (a) L-VOD, (b) IB-VOD, (c) LPDR-VOD, (d) liu-VOD, (e) NDVI, (f) EVI, (g) LAI, and (h) tree cover for the whole biomes. R_1 represents the spatial correlation between VIs/VODs and Saatchi AGB, R_2 represents the spatial correlation between VIs/VODs estimated AGBs and Saatchi AGB. All the correlations are significant considering the criteria $p < 0.05$.

ranging from 0.80 to 0.93, and a median *RMSD* value of 23.90 Mg/ha ranging from 17.34 to 31.70 Mg/ha (Table 3). Following tree cover product, LAI estimated AGBs showed lower correlation values ($R_2 = 0.62$–0.80) with reference AGBs. It can be seen that the correlation values obtained by NDVI and EVI estimated AGBs were the lowest ($R_2 = 0.49$–0.75), with *RMSD* ranging from 23.40–47.70 Mg/ha (Figures 3 (e–f) and Figure S2(E)-(F)).

With respect to VODs, the best estimation results were obtained from L-VOD ($R_2 = 0.79$–0.88) and LPDR-VOD ($R_2 = 0.76$–0.90), followed by IB-VOD ($R_2 = 0.72$–0.86) and Liu-VOD ($R_2 = 0.65$–0.81) (Figure 3(a–d) and Figure S2(A)-(D)). Considering both the R_2 and *RMSD* metrics, it can be observed that L-VOD and LPDR-VOD estimated AGBs have almost comparable performance, with a median R_2 of 0.83 and 0.82 and *RMSD* of 27.30 and 26.80 Mg/ha, respectively.

4.2.2. Different land cover types

To understand the sensitivity of VIs and VODs to reference AGB over the different land cover types,

we compared the VIs and VODs with AGB for forest, shrubland, grassland, and cropland, respectively. The relationship between VIs/VODs and AGB estimated from six reference AGB maps is shown in Figures 4–6 (with Saatchi) and Figure S3-S6 (with Baccini, CCI, Saatchi-WT, Saatchi-RF, and Su) for different land cover types.

Over forest, it can be seen that tree cover and IB-VOD estimated AGBs have the highest correlation values (with median R_2 value of 0.60 and 0.61) and lowest *RMSD* (with median *RMSD* value of 34.30 and 34.25 Mg/ha) with reference AGBs (Figure 4 and Figure S3). LPDR-VOD estimated AGBs ranked the third highest correlation values (with a median R_2 value of 0.57, median *RMSD* value of 35.62 Mg/ha) with reference AGBs, and presented a better performance than other VIs (LAI, NDVI, and EVI) estimated AGBs ($R_2 = 0.31$–0.32, *RMSD* = 40.58–40.95 Mg/ha) and other VODs (L-VOD and Liu-VOD) estimated AGBs ($R_2 = 0.23$–0.33, *RMSD* = 40.99–41.56 Mg/ha). However, our results showed that the VIs and VODs have a lower sensitivity to AGB in forest, relative to in other three land cover classes.

Table 3. Spatial correlation (R_2) between VIs/VODs estimated AGBs and reference AGBs computed using the logistic regression. All the correlations are significant considering the criteria $p < 0.05$.

| Products	L-VOD	IB-VOD	LPDR-VOD	Liu-VOD	NDVI	EVI	LAI	Tree Cover
Saatchi	0.82	0.83	0.84	0.80	0.67	0.56	0.72	0.87
Baccini	0.80	0.72	0.79	0.70	0.66	0.59	0.77	0.85
CCI	0.79	0.75	0.76	0.75	0.64	0.49	0.62	0.80
Saatchi-WT	0.85	0.85	0.87	0.84	0.73	0.62	0.75	0.90
Saatchi-RF	0.88	0.86	0.90	0.85	0.75	0.65	0.80	0.93
Su	0.79	0.78	0.79	0.76	0.62	0.53	0.69	0.83
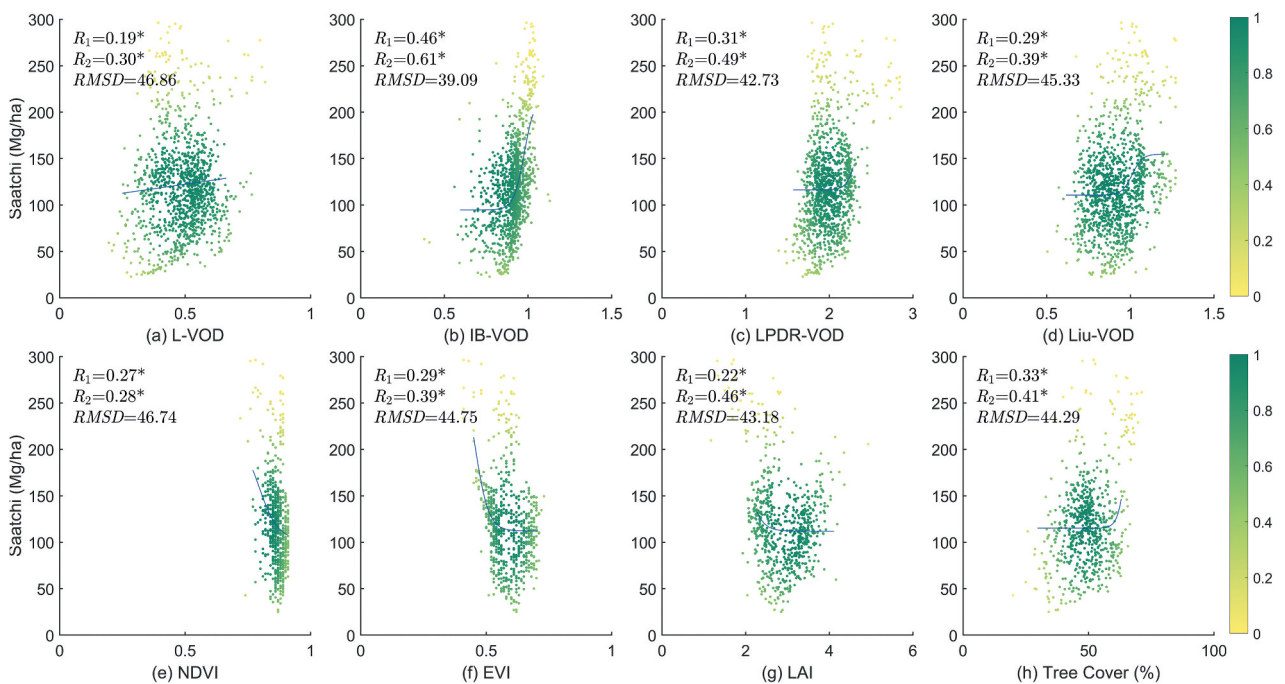
Figure 4. The spatial relationship (R_1, R_2, and *RMSD* (Mg/ha)) between Saatchi AGB and VIs/VODs from (a) L-VOD, (b) IB-VOD, (c) LPDR-VOD, (d) liu-VOD, (e) NDVI, (f) EVI, (g) LAI, and (h) tree cover for the forest. R_1 represents the spatial correlation between VIs/VODs and Saatchi AGB, R_2 represents the spatial correlation between VIs/VODs estimated AGBs and Saatchi AGB. All the correlations are significant considering the criteria $p < 0.05$.

Over shrubland, it can be observed that tree cover estimated AGBs present the highest correlation values ($R_2 = 0.74–0.89$) with reference AGBs, with *RMSD* ranging from 17.60 to 34.40 Mg/ha (Figure 5 and Figure S4). L-VOD estimated AGBs showed higher correlation values ($R_2 = 0.70–0.84$) and lower *RMSD* (16.69–36.75 Mg/ha) with reference AGBs than LPDR-VOD ($R_2 = 0.64–0.82$), IB-VOD ($R_2 = 0.60–0.75$) and Liu-VOD ($R_2 = 0.58–0.77$) in shrubland. When compared to L-VOD, both IB-VOD and LPDR-VOD still exhibit a somehow saturation effects for

AGB values >100 Mg/ha in shrubland (Figures 5(b–c) and Figure S4(B)-(C)), and the saturation is more obvious for NDVI and EVI products (Figures 5(e–f) and Figure S4(E)-(F)).

Over grassland and cropland, the relationships between VIs/VODs and reference AGBs are observed to be closer to linear (Figure 6 and Figure S5-S6). For cropland, both AGBs retrieved using L-VOD and tree cover have similar accuracy against the reference AGBs, indicated by the correlation values ($R_2 = 0.53–0.78$ for L-VOD and $R_2 = 0.54–0.77$ for tree cover). For grassland,

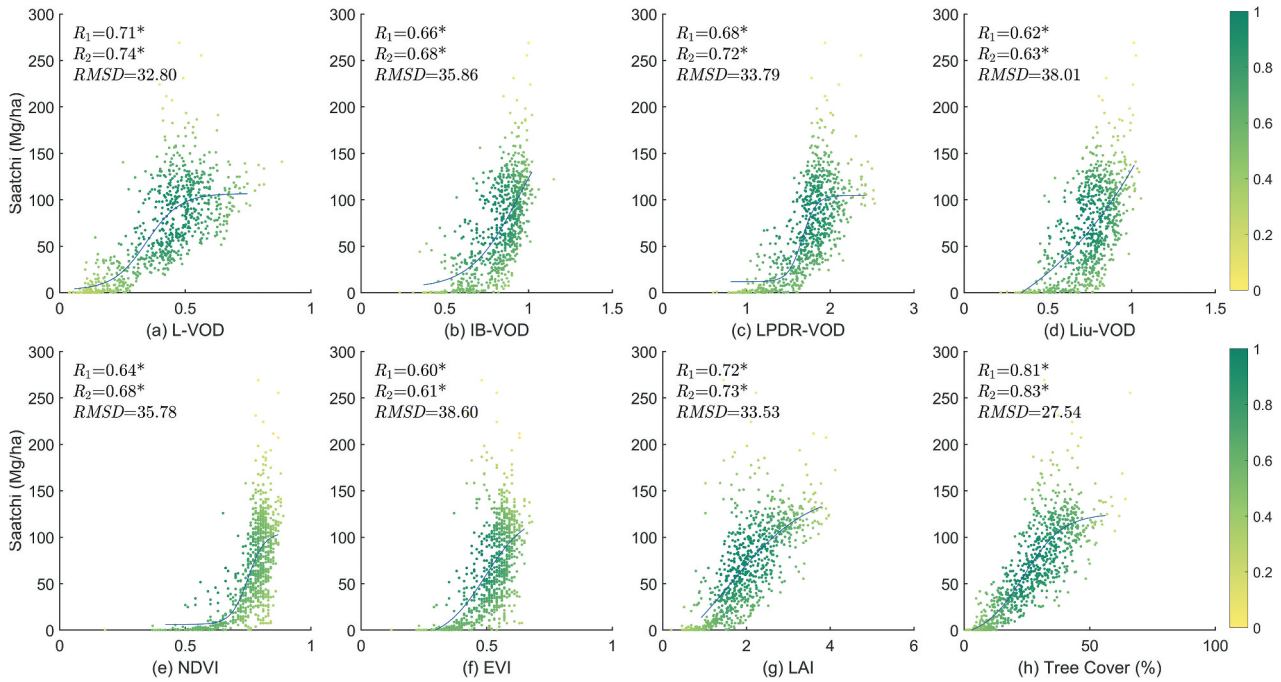**Figure 5.** Same as Figure 3 but for shrubland. All the correlations are significant considering the criteria $p < 0.05$.
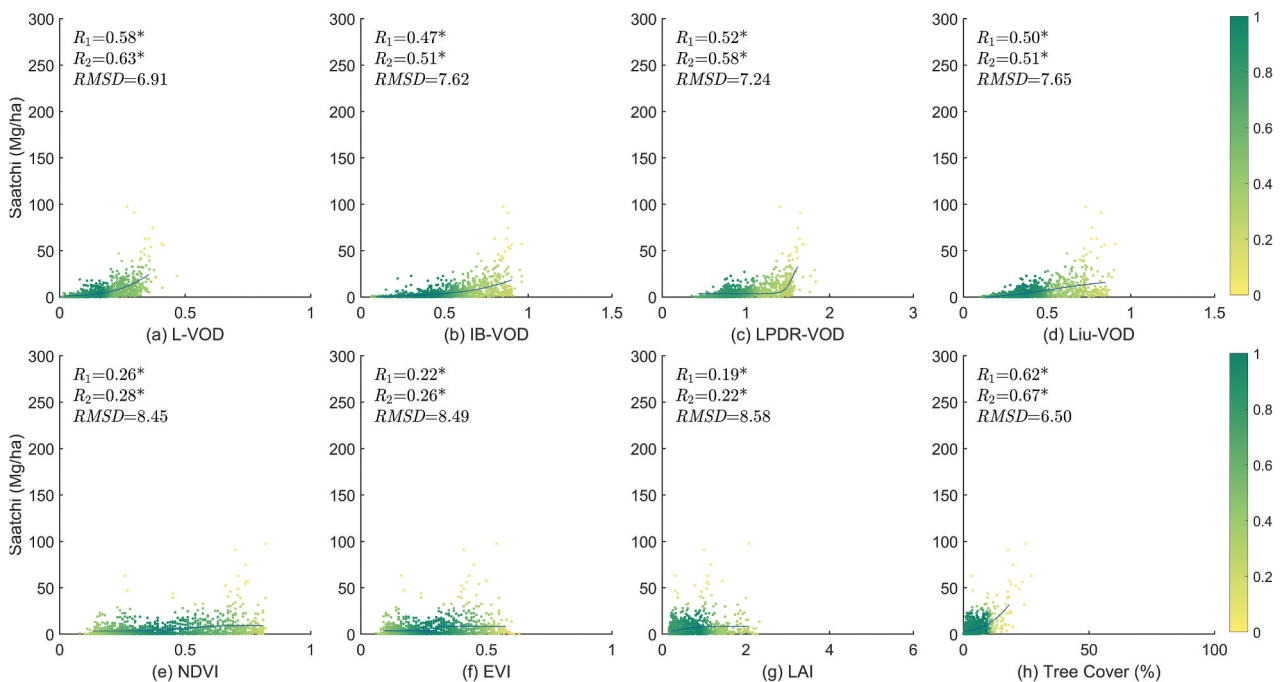

Figure 6. Same as Figure 3 but for grassland. All the correlations are significant considering the criteria $p < 0.05$.

tree cover estimated AGBs showed the best correlation values ($R_2 = 0.62$–0.69) with reference AGBs, followed by L-VOD estimated AGBs ($R_2 = 0.52$–0.68) with *RMSD* ranging from 2.64 to 15.45 Mg/ha.

Overall, the correlation values obtained by tree cover was generally the highest over most vegetation types. With respect to VODs, the best performance was achieved with IB X-VOD for forest (with median R_2 value of 0.61), and L-VOD for other three land cover classes, with median R_2 value of 0.77 for shrubland, 0.56 for grassland, and 0.57 for cropland.

4.3. Inter-comparison between VIs/VODs and AGB

To compare the performance of VIs and VODs on monitoring AGB, the median values of evaluation metrics (i.e. R_1, R_2, and *RMSD*) associated with its standard errors were summarized (Figure 7). Considering all classes altogether, the highest correlation values were obtained by tree cover (with a median value of $R_1 = 0.85$, $R_2 = 0.86$), followed by L-VOD ($R_1 = 0.80$, $R_2 = 0.83$), LPDR-VOD ($R_1 = 0.76$, $R_2 = 0.82$). NDVI ($R_1 = 0.57$, $R_2 = 0.68$) and EVI ($R_1 = 0.54$, $R_2 = 0.57$) showed the lowest correlation values and highest *RMSD* (35.23 and 39.13 Mg/ha) with reference AGBs.

Among different land cover classes, the highest correlations values between VIs/VODs and AGB can be observed in shrubland, followed by grassland, cropland, and forest (Figure 7). For forest, the highest correlation values were obtained by tree cover ($R_1 = 0.48$, $R_2 = 0.61$), followed by IB-VOD ($R_1 = 0.34$, $R_2 = 0.61$) and LPDR-VOD ($R_1 = 0.29$, $R_2 = 0.57$). Also, tree cover showed the highest correlation with reference AGBs in shrubland ($R_1 = 0.82$, $R_2 = 0.83$) and grassland ($R_1 = 0.56$, $R_2 = 0.59$). L-VOD was better correlated to reference AGBs than other three VODs in shrubland and grassland. For cropland, L-VOD and tree cover product showed similar performances ($R_1 = 0.48$, $R_2 = 0.57$ for L-VOD and $R_1 = 0.47$, $R_2 = 0.55$ for tree cover). In summary, the correlation values obtained by tree cover was generally the highest over most vegetation types (e.g. forest, shrubland, and grassland). With respect to VODs, the best performance was achieved with IB X-VOD for forest, and L-VOD for other three land cover classes. IB-VOD and Liu-VOD exhibit similar performance across various vegetation types, such as shrubland, grassland, and cropland.

To compare the performance of different reference AGB products, the median values of evaluation metrics (i.e. R_1, R_2, and *RMSD*) of associated with its standard errors were summarized by different AGBs (Figure 8). Regarding the different reference AGB maps, the best correlation values of reference AGBs with VIs and VODs were generally observed in
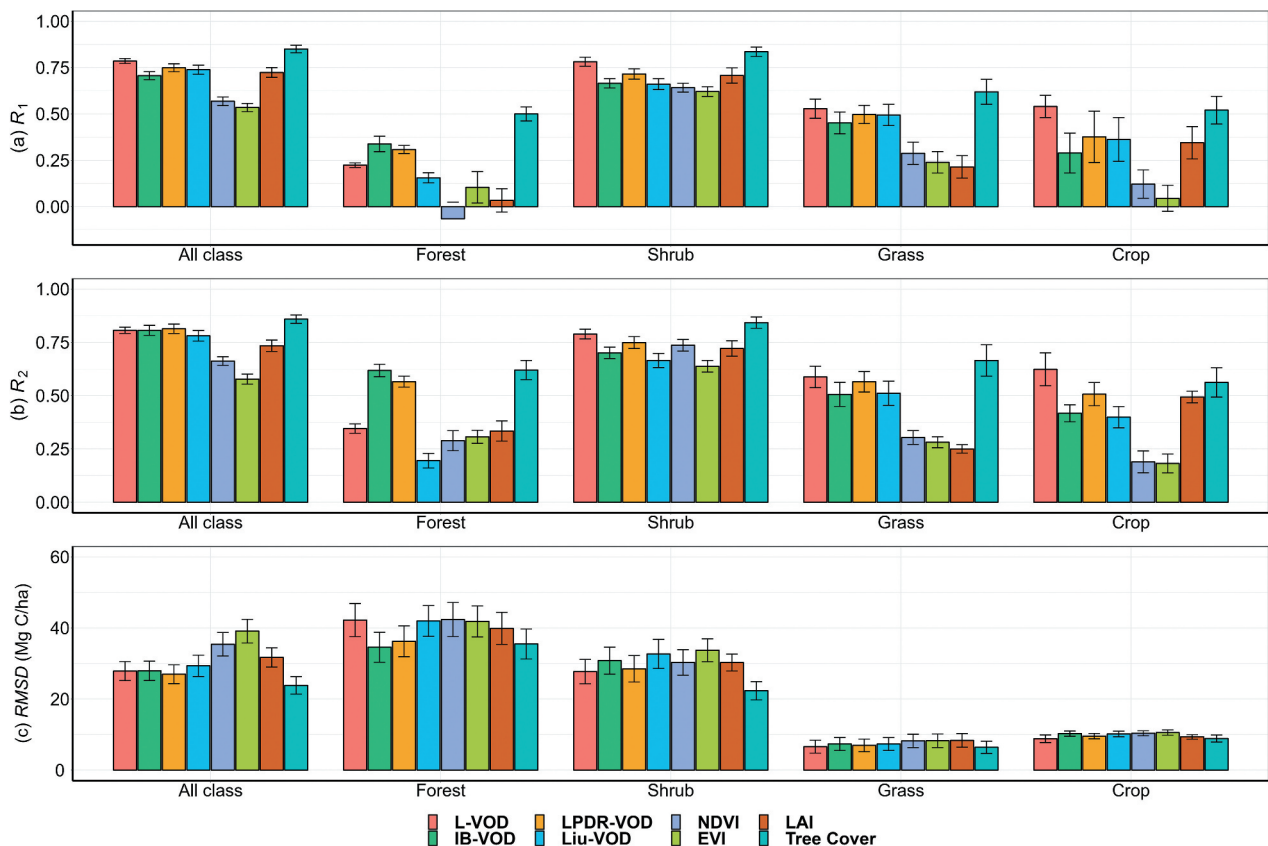

Figure 7. Comparison of median value of (a) R_1, (b) R_2, and (c) *RMSD* for the relationship between VIs/VODs and reference AGBs for different land cover classes. The error bars indicate the standard error of the metrics.
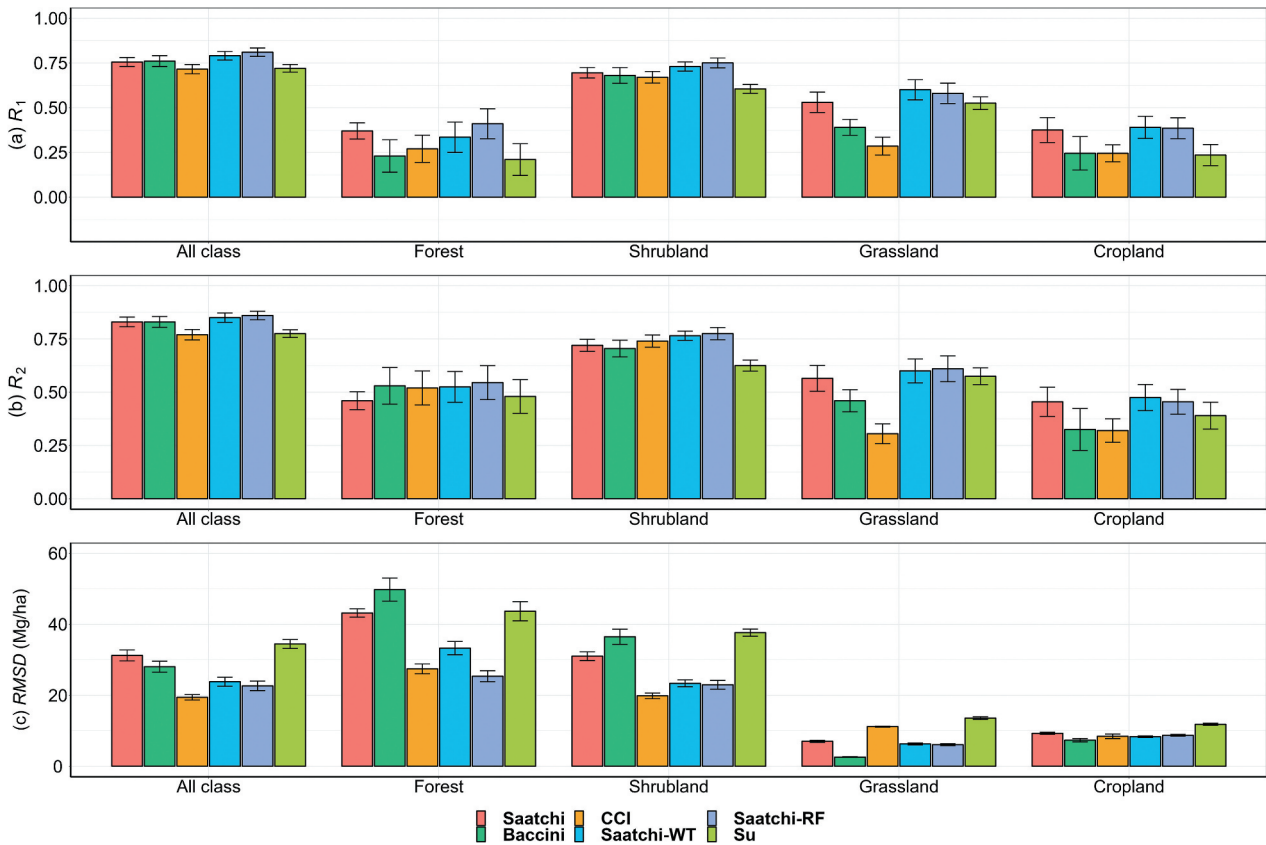
Figure 8. Comparison of median value of (a) R_1, (b) R_2, and (c) *RMSD* for the relationship between reference AGBs and VIs/VODs for different land cover classes. The error bars indicate the standard error of the metrics.

Saatchi-RF map (with a median value of $R_1 = 0.75$, $R_2 = 0.83$), followed by Saatchi-WT map (with a median value of $R_1 = 0.78$, $R_2 = 0.80$). In particular, the best correlation values of VIs/VODs estimated AGBs and reference AGBs were found with (1) Saatchi-WT map for forest, grassland, and cropland (with a median R_2 of 0.45, 0.50, and 0.44, respectively). (2) Saatchi-RF map (with a median R_2 of 0.78) for shrubland.

5. Discussion

5.1. Sensitivity of VIs to AGB

It is noted that the correlations obtained by tree cover were generally the highest over most vegetation types (e.g. forest, shrubland, and grassland) (Figure 7). This suggests that tree cover product could well capture the spatial patterns of AGB. However, the possible reasons for this may partly be explained by the fact that the tree cover product is not independent from the reference AGBs, given that the other VIs such as NDVI, EVI, and LAI, were as input for the retrieval of reference AGBs (Baccini et al. 2012; Saatchi et al. 2011; Su et al. 2016), and these VIs and tree cover are all derived from MODIS reflectance bands. Compared to the ground reference data, previous studies showed that the MODIS tree cover product was substantially overestimated in croplands in regions, such as South America (Qin et al. 2017) and Southeast Asia

(Leinenkugel et al. 2015). More accuracy assessments are needed to understand the tree cover uncertainties besides the assessment in Maryland and Brazil. The annual MODIS tree cover product is the averaged tree cover products generated by 30 image-based decision tree algorithms. Annual tree cover maps may not be comparable at a given pixel. Thus, analyzing MODIS tree cover changes at a given pixel in time series should be cautious (Leinenkugel et al. 2015).

Our results indicated that optical VIs such as NDVI and EVI have low correlations with reference AGBs, and saturated obviously over dense vegetation (e.g. forest and shrubland) with AGB values higher than 50 Mg/ha (Figures 3 and 4), in agreement with previous studies (Grant et al. 2016; Rodríguez-Fernández et al. 2018). These results are likely to be related to the fact that NDVI and EVI are sensible to the green vegetation cover, which may not be strongly correlated with the total AGB in dense vegetation (Huete et al. 2002).

5.2. Sensitivity of VODs to AGB

Our results showed that the spatial correlation between L-VOD and reference AGBs are higher than other VODs (Figure 7). This is due to that the VOD retrieved at L-band has a strong penetration capacity because of the long wavelength, and is therefore more

strongly correlated with vegetation characteristics of the entire canopy layer, including the woody component (Fan et al. 2019; Li et al. 2020; Wigneron et al. 2021). This is also in agreement with Li et al. (2021) findings which showed L-VOD are better correlated with Saatchi AGB ($R_1 = 0.79$, $R_2 = 0.83$) than higher frequency VOD (e.g. X-VOD and C-VOD) products at global scale.

Note that both of the IB-VOD and LPDR-VOD trended to saturate with AGB values higher than 100 Mg/ha (Figures 3 and 4). This result supports the findings of Chaparro et al. (2019), who found VOD at higher frequencies (e.g. X-band and C-band), as well as optical indices, saturated in dense vegetation of tropic. This may lead to the uncertainties of AGB estimation using IB-VOD and LPDR-VOD in tropical forests of southern China. It is worth noting that the IB-VOD and LPDR-VOD products are particularly responsive to the top layer of the vegetation in the canopy, which makes them well-suited for tracking seasonal fluctuations in the green vegetation components in areas with less dense vegetation (Frappart et al. 2020; Li et al. 2021). Moreover, X-VOD are less affected by RFI and available for long-term time series relative to L-VOD, which can provide effective global monitoring of vegetation trends (Du et al. 2017; Liu et al. 2015; Moesinger et al. 2020).

Our results showed that L-VOD has a low sensitivity to AGB over the forest lands, relative to IB-VOD and LPDR-VOD (Figure 7). This can be partly explained by that the effects of RFI on L-VOD over China are generally strong (Fernandez-Moran et al. 2017), especially in southern China where tropical and subtropical forests are mainly dominant (Figure S7), which could consequently decrease the performance of L-VOD on monitoring forest AGB in China. It should be noted that the impact of RFI on L-VOD has significantly decreased over China in recent years (Wigneron et al. 2021). Due to the relatively large pixel size (0.25°), a pixel may contain heterogeneity and include multiple land cover classes (e.g. forests, shrubs), which may also affect the performance of VODs for specific land cover class (Gevaert et al. 2016). To ensure the relatively homogeneous land cover conditions, only pixels with a dominant fraction of single class higher than 80% are considered. On the other hand, the different temporal coverages and gaps between the datasets could also affect the performance of the comparison. Thus, the sensitivity to AGB were estimated by comparing the reference AGBs with average value of VOD and VIs. Our results showed that the best correlations of reference AGBs and VODs were generally found in Saatchi-RF maps and Saatchi-WT maps (Figure 8). This could be attributed to the fact that the two hybrid AGB maps (i.e. WT and RF)

showed better agreement with the ground observations (Supplementary Text) (Tang et al. 2018). Recently, a refined SMOS multi-angular brightness temperature dataset spanning over a decade was generated based on a two-step regression approach, providing opportunities for retrieving land parameters such as VOD and soil moisture (Peng et al. 2023; Zhao et al. 2015). The synergistic use of VOD from different frequencies could provide a more comprehensive assessment of dynamic of vegetation AGB (Chaparro et al. 2019).

6. Conclusions

In this study, we evaluated the performance of four optical VIs (NDVI, EVI, LAI, and tree cover) and microwave-derived VODs (L-VOD, IB-VOD, LPDR-VOD, and Liu-VOD) for monitoring AGB across China. Tree cover was found to have the highest correlation (median R value of 0.85) with reference AGBs over most vegetation types (e.g. forest, shrubland, and grassland). Since L-VOD is more responsive to non-green vegetation components such as trunks and branches, thus showing higher correlation (median R values of 0.80) with reference AGBs than the other VODs in China. However, L-VOD was found to have lower correlations with reference AGBs than IB-VOD and LPDR-VOD in forest, which are mostly due to the effects of RFI on L-VOD over China are generally strong (Wigneron et al. 2021). Among the six reference AGB products, Saatchi-WT and Saatchi-RF were found to be better correlated with VIs and VODs than other AGB products.

This study provides the first comprehensive assessment of optical VIs and microwave VODs on monitoring AGB in China. The findings of this study suggested that L-VOD is a promising index for monitoring AGB stocks and dynamics in China. X-VOD is highly responsive to the green vegetation components, making it suitable for tracking temporal changes in vegetation at the top of the canopy (Frappart et al. 2020). It is valuable to synthesis these products to provide a more comprehensive assessment of the dynamics of vegetation (Mateo-Sanchis et al. 2019; Prigent and Jimenez 2021; Zhang et al. 2022). We expect our findings could enhance the accuracy of VOD retrieval algorithms and help to select the suitable VOD products to monitor AGB dynamics in China.

Disclosure statement

No potential conflict of interest was reported by the author(s).

Notes on contributors

Zhongbing Chang received his PhD from the South China Botanical Garden, Chinese Academy of Sciences. He is the engineer of Surveying and Mapping Institute Lands and Resource Department of Guangdong Province. He developed a methodology to estimate the distribution and dynamics of forest aboveground carbon stock in China by integrating optical vegetation indices and microwave VOD remote sensing products.

Lei Fan is awarded the National Science Fund for Excellent Young Scholar for his achievements in the area of remote sensing of global forest change. He is a PHD supervisor of Southwest University. He is engaged in passive microwave remote sensing monitoring technology for forest carbon stocks and revealing the response mechanism of carbon sinks for climate change. He led the research of the first low-frequency passive microwave (L-VOD)-based forest carbon stock products.

Jean-Pierre Wigneron is a senior research scientist at the INRAE. His main interest is in the use of passive and active microwave remote sensing to monitor the carbon and water cycles of forest areas. He developed pioneering work in the simultaneous retrievals of soil moisture and vegetation biomass from passive microwave remote sensing observations and developed the L-MEB model, a forward model of operational algorithms for the SMOS satellite mission. He coordinated the development of several VOD from satellite missions (SMOS, ASCAT, AMSRE/2, SMAP) which are now recognized as major tools in monitoring forest carbon stocks at continental scales.

Ying-Ping Wang is a chief research scientist in CSIRO and one of the two key scientists responsible for developing the Australian community land surface model (CABLE). His major achievements include the development of the CABLE model, two-leaf canopy scheme, the unified theory of global nitrogen fixation, and the first global model of carbon, nitrogen and phosphorus cycles. He also pioneered the applications of model-data fusion in terrestrial ecology. He is chief editor for *Agriculture and Forest Meteorology* since 2019.

Xiaojun Li is working on the topic of "Improvement of the SMOS-IC retrievals of soil moisture and vegetation L-VOD index" at the INRAE, Bordeaux. He is engaged in microwave soil moisture/VOD retrieval models, validation, and carbon cycle estimation. He developed the SMOS-IC version 2 (V2) retrieval product, and is currently responsible for the evaluation and release of the SMOS-IC V2 products.

Mengjia Wang is working on the vegetation optical depth (VOD) retrievals. She developed the AMSR2 IB VOD, which is a passive X-band VOD product retrieved from AMSR2 brightness temperature observations.

Xiangzhuo Liu is working on the vegetation optical depth (VOD) retrievals. He developed the ASCAT IB VOD, which is a active C-band VOD product retrieved from ASCAT brightness temperature observations.

Huan Wang received her PhD from the College of Urban and Environmental Sciences, Peking University. She is engaged in passive microwave remote sensing monitoring technology for forest carbon stocks and revealing the response mechanism of carbon sinks for climate change.

Tianxiang Cui is a Master's supervisor of Nanjing Forestry University. He is engaged in remote sensing of terrestrial vegetation productivity, and daylight-induced chlorophyll fluorescence.

Ling Yu received her PhD from Southwest university. Her major is Cartography and Geographic Information System. Her research focuses on the applications of remote sensing and GIS in forest disturbance and carbon dynamics in boreal forests.

Jianping Wu is an Associate Researcher at the Guangzhou Institute of Geography, Guangdong Academy of Sciences. His research interests encompass Global Ecology, Ecosystem Ecology, Urban Ecosystem, and Forest Ecosystem. He is engaged in investigating the impact and mechanisms of global climate change on soil carbon cycling processes.

Xin Xiong is working in the Lushan Botanical Garden, Chinese Academy of Sciences. His research interests include global change ecology and forest ecology, with a focus on carbon cycling processes and mechanisms in subtropical forest ecosystems. He is the group leader of the ecosystem ecology research group (Associate Researcher) and is a Master's supervisor at Nanchang University and Anhui Agricultural University. He is also an Executive Director of the Jiangxi Botanical Society.

Shuo Zhang is the leader of Forestry Policy Research Office, Center for Zhaoqing High-level Talent Development and is the specially appointed research fellow of Guangdong Center of South China National Forest Reserve Research Center. He is engaged in the microbial regulations on soil carbon accumulation during forest restoration.

Xuli Tang is engaged in the research of forest ecosystem processes and response to global change. She is working on the project of mechanisms of carbon accumulation in forest ecosystems of different maturity levels in the South Asian tropics. Her project "Mechanisms of carbon, nitrogen and water evolution during the restoration/succession of tropical subtropical forest ecosystems in South China" won the second prize of the National Natural Science Award.

Junhua Yan is awarded the National Science Fund for Distinguished Young Scholars for his achievements in the area of land surface ecological processes and environmental changes. He is a PHD supervisor of the South China Botanical Garden, Chinese Academy of Sciences. He developed a novel methodology to estimate land surface carbon sequestration within the subsurface area, proposed a new driving mechanism for land surface carbon sequestration in monsoon regions, and elucidated the effects of environmental changes in China's tropical and subtropical regions on land surface carbon sequestration.

ORCID

Zhongbing Chang 🔟 http://orcid.org/0000-0003-1470-6939
Lei Fan 🔟 http://orcid.org/0000-0002-1834-5088
Jean-Pierre Wigneron 🔟 http://orcid.org/0000-0001-5345-3618
Ying-Ping Wang 🔟 http://orcid.org/0000-0002-4614-6203
Junhua Yan 🔟 http://orcid.org/0000-0002-9948-2358

Data availability statement

L-VOD and IB-VOD product were downloaded from the SMOS-IC website (https://ib.remote-sensing.inrae.fr/). LPDR-VOD product was downloaded from National Snow and Ice Data Center (https://nsidc.org/data/nsidc-0451/). Liu-VOD product was downloaded from Australian National University (https://wald.anu.edu.au/data/). MODIS products were downloaded from the LP DAAC (https://ladsweb.modaps.eosdis.nasa.gov/).

References

Baccini, A., S. J. Goetz, W. S. Walker, N. T. Laporte, M. Sun, D. Sulla-Menashe, J. Hackler, et al. 2012. "Estimated Carbon Dioxide Emissions from Tropical Deforestation Improved by Carbon-Density Maps." *Nature Climate Change* 2:182–185. https://doi.org/10.1038/nclimate1354.

Baccini, A., W. Walker, L. Carvalho, M. Farina, D. Sulla-Menashe, and R. A. Houghton. 2017. "Tropical Forests are a Net Carbon Source Based on Aboveground Measurements of Gain and Loss." *Science* 358:230–234. https://doi.org/10.1126/science.aam5962.

Blackard, J., M. Finco, E. Helmer, G. Holden, M. Hoppus, D. Jacobs, A. Lister, G. Moisen, M. Nelson, and R. Riemann. 2008. "Mapping U.S. Forest Biomass Using Nationwide Forest Inventory Data and Moderate Resolution Information." *Remote Sensing of Environment* 112:1658–1677. https://doi.org/10.1016/j.rse.2007.08.021.

Brandt, M., J. P. Wigneron, J. Chave, T. Tagesson, J. Penuelas, P. Ciais, K. Rasmussen, et al. 2018. "Satellite Passive Microwaves Reveal Recent Climate-Induced Carbon Losses in African Drylands." *Nature Ecololy & Evolution* 2 (5): 827–835. https://doi.org/10.1038/s41559-018-0530-6.

Carreiras, J. M. B., S. Quegan, T. Le Toan, D. Ho Tong Minh, S. S. Saatchi, N. Carvalhais, M. Reichstein, and K. Scipal. 2017. "Coverage of High Biomass Forests by the ESA BIOMASS Mission Under Defense Restrictions." *Remote Sensing of Environment* 196:154–162. https://doi.org/10.1016/j.rse.2017.05.003.

Chang, Z., L. Fan, J.-P. Wigneron, Y.-P. Wang, P. Ciais, J. Chave, R. Fensholt, et al. 2023. "Estimating Aboveground Carbon Dynamic of China Using Optical and Microwave Remote-Sensing Datasets from 2013 to 2019." *Journal of Remote Sensing* 3:0005. https://doi.org/10.34133/remotesensing.0005.

Chang, Z., S. Hobeichi, Y.-P. Wang, X. Tang, G. Abramowitz, Y. Chen, N. Cao, et al. 2021. "New Forest Aboveground Biomass Maps of China Integrating Multiple Datasets." *Remote Sensing* 13:2892. https://doi.org/10.3390/rs13152892.

Chaparro, D., G. Duveiller, M. Piles, A. Cescatti, M. Vall-Llossera, A. Camps, and D. Entekhabi. 2019. "Sensitivity of L-Band Vegetation Optical Depth to Carbon Stocks in Tropical Forests: A Comparison to Higher Frequencies and Optical Indices." *Remote Sensing of Environment* 232:111303. https://doi.org/10.1016/j.rse.2019.111303.

Chen, J. M., and T. Black. 1992. "Defining leaf area index for non-flat leaves." *Plant, Cell & Environment* 15:421–429. https://doi.org/10.1111/j.1365-3040.1992.tb00992.x.

Chen, J. M., W. Ju, P. Ciais, N. Viovy, R. Liu, Y. Liu, and X. Lu. 2019. "Vegetation Structural Change Since 1981 Significantly Enhanced the Terrestrial Carbon Sink." *Nature Communications* 10:4259. https://doi.org/10.1038/s41467-019-12257-8.

Chen, Y., X. Feng, B. Fu, H. Ma, C. M. Zohner, T. W. Crowther, Y. Huang, X. Wu, and F. Wei. 2023. "Maps with 1km Resolution Reveal Increases in Above- and Belowground Forest Biomass Carbon Pools in China Over the Past 20 Years." *Earth System Science Data* 15:897–910. https://doi.org/10.5194/essd-15-897-2023.

Cui, T., L. Fan, P. Ciais, R. Fensholt, F. Frappart, S. Sitch, J. Chave, et al. 2023. "First Assessment of Optical and Microwave Remotely Sensed Vegetation Proxies in Monitoring Aboveground Carbon in Tropical Asia." *Remote Sensing of Environment* 293:113619. https://doi.org/10.1016/j.rse.2023.113619.

Didan, K. 2015. *MOD13A3 MODIS/Terra Vegetation Indices Monthly L3 Global 1km Sin Grid v006.* NASA EOSDIS Land Processes Distributed Active Archive Center.

Dimiceli, C., M. Carroll, R. Sohlberg, D. Kim, M. Kelly, and J. Townshend. 2015. MOD44B *MODIS/Terra Vegetation Continuous Fields Yearly L3 Global 250 M SIN Grid V006.* NASA EOSDIS Land Processes Distributed Active Archive Center.

Dou, Y., F. Tian, J.-P. Wigneron, T. Tagesson, J. Du, M. Brandt, Y. Liu, L. Zou, J. S. Kimball, and R. Fensholt. 2023. "Reliability of Using Vegetation Optical Depth for Estimating Decadal and Interannual Carbon Dynamics." *Remote Sensing of Environment* 285:113390. https://doi.org/10.1016/j.rse.2022.113390.

Du, J., J. S. Kimball, L. A. Jones, Y. Kim, J. Glassy, and J. D. Watts. 2017. "A Global Satellite Environmental Data Record Derived from AMSR-E and AMSR2 Microwave Earth Observations." *Earth System Science Data* 9:791–808. https://doi.org/10.5194/essd-9-791-2017.

Entekhabi, D., H. R. Reichle, D. R. Koster, and T. W. Crow. 2010. "Performance metrics for soil moisture retrievals and application requirements." *Journal of Hydrometeorology* 11 (3): 832–840. https://doi.org/10.1175/2010JHM1223.1.

ESA. 2017. Land Cover CCI Product User Guide Version 2. maps.elie.ucl.ac.be/CCI/viewer/download/ESACCI-LC-Ph2-PUGv2_2.0.pdf.

Fan, L., J.-P. Wigneron, P. Ciais, J. Chave, M. Brandt, S. Sitch, C. Yue, et al. 2023. "Siberian Carbon Sink Reduced by Forest Disturbances." *Nature Geoscience* 16:56–62. https://doi.org/10.1038/s41561-022-01087-x.

Fan, L., J. P. Wigneron, P. Ciais, J. Chave, M. Brandt, R. Fensholt, S. S. Saatchi, et al. 2019. "Satellite-Observed Pantropical Carbon Dynamics." *Nature Plants* 5:944–951. https://doi.org/10.1038/s41477-019-0478-9.

Fang, J., G. Yu, L. Liu, S. Hu, and F. S. Chapin. 2018. "Climate Change, Human Impacts, and Carbon Sequestration in China." *Proceedings of the National Academy of Sciences of the United States of America* 115 (16): 4015–4020. https://doi.org/10.1073/pnas.1700304115.

Fernandez-Moran, R., A. Al-Yaari, A. Mialon, A. Mahmoodi, A. Al Bitar, G. De Lannoy, N. Rodriguez-

Fernandez, E. Lopez-Baeza, Y. Kerr, and J.-P. Wigneron. 2017. "SMOS-IC: An Alternative SMOS Soil Moisture and Vegetation Optical Depth Product." *Remote Sensing* 9 (5): 457. https://doi.org/10.3390/rs9050457.

Frappart, F., J.-P. Wigneron, X. Li, X. Liu, A. Al-Yaari, L. Fan, M. Wang, et al. 2020. "Global Monitoring of the Vegetation Dynamics from the Vegetation Optical Depth (VOD): A Review." *Remote Sensing* 12 (18): 2915. https://doi.org/10.3390/rs12182915.

Gevaert, A. I., R. M. Parinussa, L. J. Renzullo, A. I. J. M. van Dijk, and R. A. M. de Jeu. 2016. "Spatio-Temporal Evaluation of Resolution Enhancement for Passive Microwave Soil Moisture and Vegetation Optical Depth." *International Journal of Applied Earth Observation and Geoinformation* 45:235–244. https://doi.org/10.1016/j.jag.2015.08.006.

Grant, J. P., J. P. Wigneron, R. A. M. De Jeu, H. Lawrence, A. Mialon, P. Richaume, A. Al Bitar, M. Drusch, M. J. E. van Marle, and Y. Kerr. 2016. "Comparison of SMOS and AMSR-E Vegetation Optical Depth to Four MODIS-Based Vegetation Indices." *Remote Sensing of Environment* 172:87–100. https://doi.org/10.1016/j.rse.2015.10.021.

Hansen, M., R. DeFries, J. Townshend, M. Carroll, C. Dimiceli, and R. Sohlberg. 2003. "Global Percent Tree Cover at a Spatial Resolution of 500 Meters: First Results of the MODIS Vegetation Continuous Fields Algorithm." *Earth Interactions* 7 (10): 1–15. https://doi.org/10.1175/1087-3562(2003)007<0001:GPTCAA>2.0.CO;2.

Harris, N. L., D. A. Gibbs, A. Baccini, R. A. Birdsey, S. de Bruin, M. Farina, L. Fatoyinbo, et al. 2021. "Global maps of twenty-first century forest carbon fluxes." *Nature Climate Change* 11 (3): 234–240. https://doi.org/10.1038/s41558-020-00976-6.

Hmimina, G., E. Dufrene, J. Y. Pontailler, N. Delpierre, M. Aubinet, B. Caquet, A. de Grandcourt, et al. 2013. "Evaluation of the Potential of MODIS Satellite Data to Predict Vegetation Phenology in Different Biomes: An Investigation Using Ground-Based NDVI Measurements." *Remote Sensing of Environment* 132:145–158. https://doi.org/10.1016/j.rse.2013.01.010.

Houghton, R. A. 2005. "Aboveground Forest Biomass and the Global Carbon Balance." *Global Change Biology* 11 (6): 945–958. https://doi.org/10.1111/j.1365-2486.2005.00955.x.

Huang, H., C. Liu, X. Wang, X. Zhou, and P. Gong. 2019. "Integration of Multi-Resource Remotely Sensed Data and Allometric Models for Forest Aboveground Biomass Estimation in China." *Remote Sensing of Environment* 221:225–234. https://doi.org/10.1016/j.rse.2018.11.017.

Huang, W. L., W. K. Min, J. Q. Ding, Y. C. Liu, Y. Hu, W. J. Ni, and H. F. Shen. 2022. "Forest Height Mapping Using Inventory and Multi-Source Satellite Data Over Hunan Province in Southern China." *Forest Ecosystems* 9:100006. https://doi.org/10.1016/j.fecs.2022.100006.

Huete, A., K. Didan, T. Miura, E. P. Rodriguez, X. Gao, and L. G. Ferreira. 2002. "Overview of the Radiometric and Biophysical Performance of the MODIS Vegetation Indices." *Remote Sensing of Environment* 83 (1–2): 195–213. https://doi.org/10.1016/s0034-4257(02)00096-2.

Jiang, X., A. D. Ziegler, S. Liang, D. Wang, and Z. Zeng. 2022. "Forest Restoration Potential in China: Implications for Carbon Capture." *Journal of Remote Sensing* 2022:0006. https://doi.org/10.34133/remotesensing.0006.

Jones, M. O., L. A. Jones, J. S. Kimball, and K. C. McDonald. 2011. "Satellite Passive Microwave Remote Sensing for Monitoring Global Land Surface Phenology." *Remote Sensing of Environment* 115 (4): 1102–1114. https://doi.org/10.1016/j.rse.2010.12.015.

Kim, Y., J. S. Kimball, J. Glassy, and J. Du. 2017. "An Extended Global Earth System Data Record on Daily Landscape Freeze–Thaw Status Determined from Satellite Passive Microwave Remote Sensing." *Earth System Science Data* 9 (1): 133–147. https://doi.org/10.5194/essd-9-133-2017.

Lawrence, H., J.-P. Wigneron, P. Richaume, N. Novello, J. Grant, A. Mialon, A. Al Bitar, et al. 2014. "Comparison Between SMOS Vegetation Optical Depth Products and MODIS Vegetation Indices Over Crop Zones of the USA." *Remote Sensing of Environment* 140:396–406. https://doi.org/10.1016/j.rse.2013.07.021.

Leinenkugel, P., M. L. Wolters, N. Oppelt, and C. Kuenzer. 2015. "Tree Cover and Forest Cover Dynamics in the Mekong Basin from 2001 to 2011." *Remote Sensing of Environment* 158:376–392. https://doi.org/10.1016/j.rse.2014.10.021.

Li, W., P. Ciais, S. S. Peng, C. Yue, Y. L. Wang, M. Thurner, S. S. Saatchi, et al. 2017. "Land-Use and Land-Cover Change Carbon Emissions Between 1901 and 2012 Constrained by Biomass Observations." *Biogeosciences* 14 (22): 5053–5067. https://doi.org/10.5194/bg-14-5053-2017.

Li, X., A. Al-Yaari, M. Schwank, L. Fan, F. Frappart, J. Swenson, and J. P. Wigneron. 2020. "Compared Performances of SMOS-IC Soil Moisture and Vegetation Optical Depth Retrievals Based on Tau-Omega and Two-Stream Microwave Emission Models." *Remote Sensing of Environment* 236:111502. https://doi.org/10.1016/j.rse.2019.111502.

Li, X., J.-P. Wigneron, F. Frappart, L. Fan, P. Ciais, R. Fensholt, D. Entekhabi, et al. 2021. "Global-Scale Assessment and Inter-Comparison of Recently Developed/Reprocessed Microwave Satellite Vegetation Optical Depth Products." *Remote Sensing of Environment* 253:112208. https://doi.org/10.1016/j.rse.2020.112208.

Liao, Z., A. I. J. M. Van Dijk, B. He, P. R. Larraondo, and P. F. Scarth. 2020. "Woody Vegetation Cover, Height and Biomass at 25-M Resolution Across Australia Derived from Multiple Site, Airborne and Satellite Observations." *International Journal of Applied Earth Observation and Geoinformation* 93:102209. https://doi.org/10.1016/j.jag.2020.102209.

Liu, Y. Y., R. A. M. de Jeu, M. F. McCabe, J. P. Evans, and A. I. J. M. van Dijk. 2011. "Global long-term passive microwave satellite-based retrievals of vegetation optical depth." *Geophysical Research Letters* 38 (18): L18402. https://doi.org/10.1029/2011GL048684.

Liu, Y. Y., A. I. J. M. van Dijk, R. A. M. de Jeu, J. G. Canadell, M. F. McCabe, J. P. Evans, and G. J. Wang. 2015. "Recent reversal in loss of global terrestrial biomass." *Nature Climate Change* 5 (5): 470–474. https://doi.org/10.1038/nclimate2581.

Mateo-Sanchis, A., M. Piles, J. Muñoz-Marí, J. E. Adsuara, A. Pérez-Suay, and G. Camps-Valls. 2019. "Synergistic Integration of Optical and Microwave Satellite Data for Crop Yield Estimation." *Remote Sensing of Environment* 234:111460. https://doi.org/10.1016/j.rse.2019.111460.

Mialon, A., N. J. Rodríguez-Fernández, M. Santoro, S. Saatchi, S. Mermoz, E. Bousquet, and Y. H. Kerr. 2020. "Evaluation of the Sensitivity of SMOS L-VOD to

Forest Above-Ground Biomass at Global Scale." *Remote Sensing* 12 (9): 1450. https://doi.org/10.3390/rs12091450.

Moesinger, L., W. Dorigo, R. de Jeu, R. van der Schalie, T. Scanlon, I. Teubner, and M. Forkel. 2020. "The Global Long-Term Microwave Vegetation Optical Depth Climate Archive (VODCA)." *Earth System Science Data* 12 (1): 177–196. https://doi.org/10.5194/essd-12-177-2020.

Myers-Smith, I. H., J. T. Kerby, G. K. Phoenix, J. W. Bjerke, H. E. Epstein, J. J. Assmann, C. John, et al. 2020. "Complexity Revealed in the Greening of the Arctic." *Nature Climate Change* 10 (2): 106–117. https://doi.org/10.1038/s41558-019-0688-1.

Myneni, R., Y. Knyazikhin, and T. Park. 2015. *MOD15A2H MODIS/terra leaf area index/FPAR 8-day L4 global 500 m SIN grid V006*. NASA EOSDIS Land Processes Distributed Active Archive Center.

Myneni, R. B., J. Dong, C. J. Tucker, R. K. Kaufmann, P. E. Kauppi, J. Liski, L. Zhou, V. Alexeyev, and M. K. Hughes. 2001. "A Large Carbon Sink in the Woody Biomass of Northern Forests." *Proceedings of the National Academy of Sciences of the United States of America* 98 (26): 14784–14789. https://doi.org/10.1073/pnas.261555198.

Peng, Z., T. Zhao, J. Shi, Y. H. Kerr, N. J. Rodríguez-Fernández, P. Yao, and T. Che. 2023. "An RFI-suppressed SMOS L-band multi-angular brightness temperature dataset spanning over a decade (since 2010)." *Scientific Data* 10 (1): 599. https://doi.org/10.1038/s41597-023-02499-z.

Piao, S., J. Fang, P. Ciais, P. Peylin, Y. Huang, S. Sitch, and T. Wang. 2009. "The Carbon Balance of Terrestrial Ecosystems in China." *Nature* 458 (7241): 1009–1013. https://doi.org/10.1038/nature07944.

Piao, S., Y. He, X. Wang, and F. Chen. 2022. "Estimation of China's Terrestrial Ecosystem Carbon Sink: Methods, Progress and Prospects." *Science China Earth Sciences* 65 (4): 641–651. https://doi.org/10.1007/s11430-021-9892-6.

Prigent, C., and C. Jimenez. 2021. "An Evaluation of the Synergy of Satellite Passive Microwave Observations Between 1.4 and 36 GHz, for Vegetation Characterization Over the Tropics." *Remote Sensing of Environment* 257:112346. https://doi.org/10.1016/j.rse.2021.112346.

Qin, S., H. Wang, X. Li, J. Gao, J. Jin, Y. Li, J. Lu, et al. 2023. "Enhancing Landsat Image Based Aboveground Biomass Estimation of Black Locust with Scale Bias-Corrected LiDAR AGB Map and Stratified Sampling." *Geo-Spatial Information Science* 1–14. https://doi.org/10.1080/10095020.2023.2249042.

Qin, Y., X. Xiao, J. Dong, Y. Zhou, J. Wang, R. B. Doughty, Y. Chen, Z. Zou, and B. Moore. 2017. "Annual Dynamics of Forest Areas in South America During 2007–2010 at 50-M Spatial Resolution." *Remote Sensing of Environment* 201:73–87. https://doi.org/10.1016/j.rse.2017.09.005.

Qin, Y., X. Xiao, J.-P. Wigneron, P. Ciais, M. Brandt, L. Fan, X. Li, et al. 2021. "Carbon Loss from Forest Degradation Exceeds That from Deforestation in the Brazilian Amazon." *Nature Climate Change* 11 (5): 442–448. https://doi.org/10.1038/s41558-021-01026-5.

Quegan, S., L. T. Toan, J. Chave, J. Dall, J. F. Exbrayat, D. H. T. Minh, M. Lomas, et al. 2019. "The European Space Agency BIOMASS Mission: Measuring Forest Above-Ground Biomass from Space." *Remote Sensing of Environment* 227:44–60. https://doi.org/10.1016/j.rse.2019.03.032.

Rodríguez-Fernández, N. J., A. Mialon, S. Mermoz, A. Bouvet, P. Richaume, A. Al Bitar, A. Al-Yaari, M. Brandt, and T. Kaminski. 2018. "An Evaluation of SMOS L-Band Vegetation Optical Depth (L-VOD) Data Sets: High Sensitivity of L-VOD to Above-Ground Biomass in Africa." *Biogeosciences* 15 (14): 4627–4645. https://doi.org/10.5194/bg-15-4627-2018.

Rodriguez-Veiga, P., S. Quegan, J. Carreiras, H. J. Persson, J. E. S. Fransson, A. Hoscilo, D. Ziółkowski, et al. 2019. "Forest Biomass Retrieval Approaches from Earth Observation in Different Biomes." *International Journal of Applied Earth Observation and Geoinformation* 77:53–68. https://doi.org/10.1016/j.jag.2018.12.008.

Saatchi, S. S., N. L. Harris, S. Brown, M. Lefsky, E. T. Mitchard, W. Salas, B. R. Zutta, et al. 2011. "Benchmark Map of Forest Carbon Stocks in Tropical Regions Across Three Continents." *Proceedings of the National Academy of Sciences of the United States of America* 108 (24): 9899–9904. https://doi.org/10.1073/pnas.1019576108.

Santoro, M., O. Cartus, N. Carvalhais, D. M. A. Rozendaal, V. Avitabile, A. Araza, S. de Bruin, et al. 2021. "The Global Forest Above-Ground Biomass Pool for 2010 Estimated from High-Resolution Satellite Observations." *Earth System Science Data* 13 (8): 3927–3950. https://doi.org/10.5194/essd-13-3927-2021.

Santoro, M., O. Cartus, U. Wegmüller, S. Besnard, N. Carvalhais, A. Araza, M. Herold, J. Liang, J. Cavlovic, and M. E. Engdahl. 2022. "Global Estimation of Above-Ground Biomass from Spaceborne C-Band Scatterometer Observations Aided by LiDar Metrics of Vegetation Structure." *Remote Sensing of Environment* 279:113114. https://doi.org/10.1016/j.rse.2022.113114.

Schmidt, L., M. Forkel, R. M. Zotta, S. Scherrer, W. A. Dorigo, A. Kuhn-Régnier, R. van der Schalie, and M. Yebra. 2023. "Assessing the Sensitivity of Multi-Frequency Passive Microwave Vegetation Optical Depth to Vegetation Properties." *Biogeosciences* 20 (5): 1027–1046. https://doi.org/10.5194/bg-20-1027-2023.

Scholze, M., M. Buchwitz, W. Dorigo, L. Guanter, and S. Quegan. 2017. "Reviews and Syntheses: Systematic Earth Observations for Use in Terrestrial Carbon Cycle Data Assimilation Systems." *Biogeosciences* 14 (14): 3401–3429. https://doi.org/10.5194/bg-14-3401-2017.

Su, Y., Q. Guo, B. Xue, T. Hu, O. Alvarez, S. Tao, and J. Fang. 2016. "Spatial Distribution of Forest Aboveground Biomass in China: Estimation Through Combination of Spaceborne Lidar, Optical Imagery, and Forest Inventory Data." *Remote Sensing of Environment* 173:187–199. https://doi.org/10.1016/j.rse.2015.12.002.

Tang, X., X. Zhao, Y. Bai, Z. Tang, W. Wang, Y. Zhao, H. Wan, et al. 2018. "Carbon Pools in China's Terrestrial Ecosystems: New Estimates Based on an Intensive Field Survey." *Proceedings of the National Academy of Sciences of the United States of America* 115 (16): 4021–4026. https://doi.org/10.1073/pnas.1700291115.

Teubner, I. E., M. Forkel, M. Jung, Y. Y. Liu, D. G. Miralles, R. Parinussa, R. van der Schalie, et al. 2018. "Assessing the Relationship Between Microwave Vegetation Optical Depth and Gross Primary Production." *International Journal of Applied Earth Observation and Geoinformation* 65:79–91. https://doi.org/10.1016/j.jag.2017.10.006.

Tong, X., M. Brandt, Y. Yue, P. Ciais, M. Rudbeck Jepsen, J. Penuelas, J.-P. Wigneron, et al. 2020. "Forest management in southern China generates short term extensive

carbon sequestration." *Nature Communications* 11 (1): 129. https://doi.org/10.1038/s41467-019-13798-8.

Vittucci, C., G. Vaglio Laurin, G. Tramontana, P. Ferrazzoli, L. Guerriero, and D. Papale. 2019. "Vegetation Optical Depth at L-Band and Above Ground Biomass in the Tropical Range: Evaluating Their Relationships at Continental and Regional Scales." *International Journal of Applied Earth Observation and Geoinformation* 77:151–161. https://doi.org/10.1016/j.jag.2019.01.006.

Wang, M., L. Fan, F. Frappart, P. Ciais, R. Sun, Y. Liu, X. Li, X. Liu, C. Moisy, and J.-P. Wigneron. 2021. "An Alternative AMSR2 Vegetation Optical Depth for Monitoring Vegetation at Large Scales." *Remote Sensing of Environment* 263:112556. https://doi.org/10.1016/j.rse.2021.112556.

Wang, R. Q., G. Y. Li, Y. G. Lu, and D. S. Lu. 2023. "A Comparative Analysis of Grid-Based and Object-Based Modeling Approaches for Poplar Forest Growing Stock Volume Estimation in Plain Regions Using Airborne LIDAR Data." *Geo-Spatial Information Science* 2169199. https://doi.org/10.1080/10095020.2023.2169199.

Wigneron, J.-P., L. Fan, P. Ciais, A. Bastos, M. Brandt, J. Chave, S. Saatchi, A. Baccini, and R. Fensholt. 2020. "Tropical Forests Did Not Recover from the Strong 2015–2016 El Niño Event." *Science Advances* 6 (6): eaay4603. https://doi.org/10.1126/sciadv.aay4603.

Wigneron, J.-P., T. Jackson, P. O'neill, G. De Lannoy, P. De Rosnay, J. Walker, P. Ferrazzoli, V. Mironov, S. Bircher, and J. Grant. 2017. "Modelling the Passive Microwave Signature from Land Surfaces: A Review of Recent Results and Application to the L-Band SMOS & SMAP Soil Moisture Retrieval Algorithms." *Remote Sensing of Environment* 192:238–262. https://doi.org/10.1016/j.rse.2017.01.024.

Wigneron, J.-P., Y. Kerr, A. Chanzy, and Y.-Q. Jin. 1993. "Inversion of Surface Parameters from Passive Microwave Measurements Over a Soybean Field." *Remote Sensing of Environment* 46 (1): 61–72. https://doi.org/10.1016/0034-4257(93)90032-S.

Wigneron, J.-P., Y. Kerr, P. Waldteufel, K. Saleh, M. J. Escorihuela, P. Richaume, P. Ferrazzoli, et al. 2007. "L-Band Microwave Emission of the Biosphere (L-MEB) Model: Description and Calibration Against Experimental Data Sets Over Crop Fields." *Remote Sensing of Environment* 107 (4): 639–655. https://doi.org/10.1016/j.rse.2006.10.014.

Wigneron, J.-P., X. Li, F. Frappart, L. Fan, A. Al-Yaari, G. De Lannoy, X. Liu, M. Wang, E. Le Masson, and C. Moisy. 2021. "SMOS-IC Data Record of Soil Moisture and L-VOD: Historical Development, Applications and Perspectives." *Remote Sensing of Environment* 254:112238. https://doi.org/10.1016/j.rse.2020.112238.

Xiao, J., F. Chevallier, C. Gomez, L. Guanter, J. A. Hicke, A. R. Huete, K. Ichii, et al. 2019. "Remote Sensing of the Terrestrial Carbon Cycle: A Review of Advances Over 50 Years." *Remote Sensing of Environment* 233:111383. https://doi.org/10.1016/j.rse.2019.111383.

Xu, K. X., Y. J. Su, J. Liu, T. Y. Hu, S. Jin, and Q. Ma. 2020. "Estimation of Degraded Grassland Aboveground Biomass Using Machine Learning Methods from Terrestrial Laser Scanning Data." *Ecological Indicators* 108:105747. https://doi.org/10.1016/j.ecolind.2019.105747.

Xu, L., S. S. Saatchi, Y. Yang, Y. Yu, J. Pongratz, A. A. Bloom, K. Bowman, et al. 2021. "Changes in Global Terrestrial Live Biomass Over the 21st Century." *Science Advances* 7 (27): eabe9829. https://doi.org/10.1126/sciadv.abe9829.

Yang, Q., C. Niu, X. Liu, Y. Feng, Q. Ma, X. Wang, H. Tang, and Q. Guo. 2023. "Mapping High-Resolution Forest Aboveground Biomass of China Using Multisource Remote Sensing Data." *GIScience & Remote Sensing* 60 (1): 2203303. https://doi.org/10.1080/15481603.2023.2203303.

Yang, Y., Y. Shi, W. Sun, J. Chang, J. Zhu, L. Chen, X. Wang, et al. 2022. "Terrestrial Carbon Sinks in China and Around the World and Their Contribution to Carbon Neutrality." *Science China Life Sciences* 65 (5): 861–895. https://doi.org/10.1007/s11427-021-2045-5.

Zhang, G., S. Y. Wang, Z. W. Chen, Y. Z. Zheng, R. S. Zhao, T. Y. Wang, Y. Zhu, X. Z. Yuan, W. Wu, and W. T. Chen. 2022. "Development of China's Spaceborne SAR Satellite, Processing Strategy, and Application: Take Gaofen-3 Series as an Example." *Geo-Spatial Information Science* 1–16. https://doi.org/10.1080/10095020.2022.2124129.

Zhang, R., X. Zhou, Z. Ouyang, V. Avitabile, J. Qi, J. Chen, and V. Giannico. 2019. "Estimating Aboveground Biomass in Subtropical Forests of China by Integrating Multisource Remote Sensing and Ground Data." *Remote Sensing of Environment* 232:111341. https://doi.org/10.1016/j.rse.2019.111341.

Zhang, Y., J. Ma, S. Liang, X. Li, and J. Liu. 2022. "A Stacking Ensemble Algorithm for Improving the Biases of Forest Aboveground Biomass Estimations from Multiple Remotely Sensed Datasets." *GIScience & Remote Sensing* 59 (1): 1–16. https://doi.org/10.1080/15481603.2021.2023842.

Zhao, T., J. Shi, R. Bindlish, T. J. Jackson, Y. H. Kerr, M. H. Cosh, Q. Cui, Y. Li, C. Xiong, and T. Che. 2015. "Refinement of SMOS Multiangular Brightness Temperature Toward Soil Moisture Retrieval and Its Analysis Over Reference Targets." *IEEE Journal of Selected Topics in Applied Earth Observations and Remote Sensing* 8 (2): 589–603. https://doi.org/10.1109/JSTARS.2014.2336664.

Zhao, T., J. Shi, D. Entekhabi, T. J. Jackson, L. Hu, Z. Peng, P. Yao, S. Li, and C. S. Kang. 2021. "Retrievals of Soil Moisture and Vegetation Optical Depth Using a Multi-Channel Collaborative Algorithm." *Remote Sensing of Environment* 257:112321. https://doi.org/10.1016/j.rse.2021.112321.

Zhao, T., J. Shi, L. Lv, H. Xu, D. Chen, Q. Cui, T. J. Jackson, et al. 2020. "Soil moisture experiment in the Luan River supporting new satellite mission opportunities." *Remote Sensing of Environment* 240:111680. https://doi.org/10.1016/j.rse.2020.111680.

Zhou, X., X. Lei, C. Liu, H. Huang, C. Zhou, and C. Peng. 2019. "Re-Estimating the Changes and Ranges of Forest Biomass Carbon in China During the Past 40 years." *Forest Ecosystems* 6:51. https://doi.org/10.1186/s40663-019-0208-9.